

Article

A Comparative Computational Fluid Dynamic Study on the Effects of Terrain Type on Hub-Height Wind Aerodynamic Properties

Akintayo T. Abolude ¹  and Wen Zhou ^{2,*} 

¹ School of Energy and Environment, City University of Hong Kong, Hong Kong 00852, China; atabolude2-c@my.cityu.edu.hk

² Guy Carpenter Asia-Pacific Climate Impact Center, School of Energy and Environment, City University of Hong Kong, Hong Kong 00852, China

* Correspondence: wenzhou@cityu.edu.hk; Tel.: +852-3442-7816

Received: 10 November 2018; Accepted: 13 December 2018; Published: 28 December 2018



Abstract: The increased adoption of wind power has generated global discourse in wind energy meteorology. Studies based on turbine performances show a deviation of actual output from power curve output, thereby yielding errors irrespective of the turbine site. Understanding the cause of these errors is essential for wind power optimization, thus necessitating investigation into site-specific effects on turbine performance and operation. Therefore, Computational Fluid Dynamics simulations of hub-height wind aerodynamic properties were conducted based on the $k-\epsilon$ turbulence closure model Reynolds Averaged Navier Stokes equations for three terrains. To isolate terrain-induced effects, the same 40 m above mean sea level wind climatology was imposed on all three terrains. For the four wind directions considered, turbulence intensity (TI) was least in the offshore terrain at about 5–7% but ranged considerably higher from 4–18% for the coastal and island terrain. TI on crests also increased significantly by up to 15% upstream of wind direction for the latter terrains. Inflow angle ranged from -15° to $+15^\circ$ in both coastal and island terrains but remained at $<+1^\circ$ in the offshore terrain. Hellman exponent increased from between factors of 2–4 in the other two terrains relative to that of the offshore terrain. Wind speed-up varied from about 1.06–1.13, accounting for a range of 17–30% difference in power output from a hypothetical operational 2 MW turbine output placed in the three different terrains. Turbine loading, fatigue, efficiency, and life cycle can also be impacted by the variations noted. While adopting a site-specific power curve may help minimize errors and losses, collecting these aerodynamic data alongside wind speed and direction is the future for wind power optimization under big data and machine learning.

Keywords: site-specific effects; turbulence intensity; wind speed-up; hub-height wind shear; power output fluctuations

1. Background

Increasing installation and adoption of wind energy sources into the national grid and energy mix provides unique opportunities for the optimization of wind energy despite the challenge of wind variability. While calls for wind turbine (WT) performance data sharing has continued to persist in recent years [1], it is necessary to identify and ascertain critical parameters that can impact on turbine performance and affect power generation. Among some meteorological parameters of interest, wind speed is perhaps the most influencing factor for accurate estimates of the wind energy potential of a wind turbine [2]. Wind turbine siting (termed micro-siting) can be conducted based on observational data from a proposed site [3], extrapolation of wind speed from a known height to a select height

wind power [4], reanalysis data mapping [5], and more recently computational fluid dynamics (CFD) simulations [6,7]. The uses of CFD simulations vary widely; uses include pollutant dispersion and tracing [8], wind engineering [9], wind turbine performance studies [10], indoor ventilation and air quality studies [11], tropical cyclone and extreme weather tracking, etc. By leveraging the increased robustness offered by CFD for wind energy meteorology purposes, better aerodynamic details of terrain effects on wind speed and other turbine performance-related parameters such as shear and wake can be investigated. Surveyed literatures show a thorough analysis of wakes due to terrain, obstacles, turbine parts, and turbines on downstream wind properties.

For wind engineering, the integration of CFD into turbine performance and assessments has taken different forms. Sanderse et al. [12] studied wakes in wind farms, observing a loss of up to 40% during full-wake conditions. Similar studies on turbine wakes and the effects on downstream turbines can be found in Skakoor et al. [13], Hansen et al. [14] and Giahi & Dehkordi [15]. In Hansen et al. [14], the impact of turbulence intensity and atmospheric stability on wind power deficits (errors) due to wind turbine wakes was explored. Giahi & Dehkordi [15] based on a CFD simulation of a 2 MW National Renewable Energy Laboratory (NREL) turbine concluded that torque increased with the cube of change of rotor diameter, while aerodynamic forces increased by a square factor of change in diameter. Cai et al. [16] used a combination of the basic Blade Element Momentum (BEM) and CFD codes for modeling wind flow with respect to the turbine body itself. Alaimo et al. [17] adopted a similar approach by conducting a 3D CFD analysis on a Vertical Axis Wind Turbine (VAWT) for comparing the performance of a straight blade versus helical blade. By using variations of mesh size, mesh structure, time step, and rotational velocity, different wind turbine geometries were explored with the wind fields resolved using the Reynolds Averaged Navier Stokes (RANS) equations in the ANSYS® Fluent software v14.5. Zanon et al. [18] combined the CFD simulation of aerofoil performance and BEM for overall turbine performance to recommend operational conditions for a NREL 5 MW WT with ice accretion on some aerofoil sections. In the study, the turbine blade is discretized into a finite number of annular stream tubes and the forces acting on each blade section are computed using ANSYS CFX™ for flow resolution and ICEAC2D for the ice accretion coding. They concluded that decreasing turbine rotational speed during an icing event can improve turbine performance by up to 6% when full operation is restored (relative to the baseline operational strategy). A common point of the above highlighted studies is that the adoption and application of CFD in wind engineering stem from the aerofoil design, rotor design, blade sections and elements etc geared towards design optimization. This effectively excludes how terrain features can impact on wind reaching the blade itself. Advances made in this latter regard have conventionally likewise been focused on wind fields resolution with strong recourse on the atmospheric conditions of wind power and energy meteorology, effectively taking the view-point of a meteorologist as similarly opined by Emeis [2]. Most common of these is the suitability of extrapolation laws to describe hub-height wind properties accurately while another common theme is the ability of various CFD softwares such as ANSYS (USA), OpenFOAM (UK), WindSim (Norway) and methods such as Reynolds Averaged Navier Stokes—RANS, Direct Navier Stokes—DNS, Large Eddy Simulation—LES to accurately resolve wind flow over natural homogenous and/or complex terrains. Dhunny et al. [19] validated wind on-site measurements of wind speeds at four heights above ground level on the Island of Mauritius for which wind power estimates were obtained using WindSim. By testing four different models based on three discretization schemes in various mesh configurations, the study concluded on the suitability and appropriateness of WindSim for studying wind flow over complex terrains. Blocken et al. [20] used the RANS equations with a revised $k-\epsilon$ to estimate and validate wind speed and direction over four various types of complex terrain, obtaining 10–20% corresponding values relative to the observational measurements. Notwithstanding, the broad aim of the discussed approaches are the increased diffusion and optimization of wind energy measured through the wind turbine (farm) power output.

Wind turbine power output has been studied under themes such as performance characterization [21–23], assessment and management [24], estimation/forecast errors [25], and power curves [26–28].

One common conclusion is the presence of deviations of the actual farm or turbine output from that of the supplied power curve using the words errors, dispersion belly and/or variations interchangeably. Abolude & Zhou [24] observed deviations of actual output from the turbine power curve for an 800 kW WT, while Villaneuva & Feijoo [29] argue for a “true power curve” to minimize estimation errors observed from WT real time performance data. In another related study, Whale et al. [30] noted deviations of the actual power from manufacturer WTPC for small wind turbines at high wind speeds, and Cooney et al. [21] reported similar differences during a performance characterization study for an urban-sited wind turbine. Other discussions of errors for different terrains and layout configurations can be found in the various studies [22,27,30–33]. This phenomenon has been linked to factors including the site-specificity of WTPCs [32], the dynamic behavior of wind [34], turbine age [23], wind shear and specific weather conditions [29], and environmental and topographic conditions/terrain [26,32,33].

Wind flow over terrain can significantly affect turbine performance. Aerodynamically, the presence of obstacles such as hills, trees, buildings etc can affect the wind (fluid) flow around and over them, resulting in horizontal and or vertical changes of flow paths, direction and angles. Wind Turbine Power Curves based on wind tunnel tests and measurements show very little (if any) accommodation for the impacts of turbulence and roughness of terrain on turbine power output. In their work, Tindal et al. [35] succinctly captured this, stating that “site-specific adjustments are required by Wind TPCs (WTPCs) in order to capture the effects of turbulence, complex terrain, wind shear, blade fouling and icing, etc”. Furthermore, Lubitz [36] concluded that “current power curve representations do not account for the impact of turbulence on small turbines” when investigating the performance of a three-bladed 2.5 m diameter, 1.0 kW horizontal axis wind turbine. The task of investigating and possibly quantifying the extent of deviation arising due to terrain type and its overall impact on WT performance thus becomes imperative and urgent for the management and optimization of wind power.

One way to achieve the above task is the use of computational tools based on non-linear models of the equations of motion in CFD packages. Recently, Uchida [37] used a Large Eddy Simulation (LES) technique to show terrain-induced turbulence from a terrain feature upstream of a wind turbine and proved that this affected the downstream turbine directly. The work of Bilal et al. [38] also concluded that the Reynolds Averaged Navier Stokes (RANS) equations are capable of simulating and resolving fluid flow around or over obstacles. Thus, drawing upon the conclusions of Lydia et al. [32] on complex terrain influences on wind properties, this study takes the reported suitability of WindSim [39] to investigate turbine performance related to wind aerodynamic properties over three different terrains. The goal of the paper is to provide an answer to the question of how terrain type affects wind properties critical to turbine performance, using a RANS-based CFD simulation to resolve for wind flow from selected directions over offshore, coastal and island terrains.

2. Data and Methodology

Each terrain configuration comprises a 160 by 160 nodal structure calibrated to a local 4 km by 4 km scale as seen in Figure 1a–c. For the offshore terrain, height above mean sea level was set at 0 m with a typical calm open sea simulation while the roughness height was set to a constant value of 0.0003. The coastal terrain has a maximum peak of about 185 m above mean sea level in the northern part of the terrain, decreasing (in elevation) gradually southward to the open waters where the height is retained at 0 m. The portion of the terrain extends about 5.6 km diagonally upwards to the north-west corner of the terrain simulation. In the island terrain simulation, two hills are present with peak heights of about 106 m and 140 m above mean sea level, with a base width (widest) of about 1380 m and 750 m, respectively; thus, the lesser peaked hill had flatter slopes relative to the higher peaked hill. To ensure uniformity, the same initial and boundary conditions are forced on the three terrains despite the topographic differences. Summarily, for these conditions, the boundary layer height was set to 500 m and the boundary condition at the top of the 3D terrain was set to fixed pressure. The ground up boundary layer height was assumed to be governed by the log profile which assumes a flat terrain

is obtainable at the edges of the terrain. To overcome the possible limitations of this log profile, the virtual climatology introduced was inserted at the terrain center away from border boundary effects and the air inlet is now based on four wind directions 60° , 150° , 240° , and 330° . The virtual climatology was used as a reference point for the spatial distribution of wind properties including inlet direction and speed, to represent measurements taken 40 m above ground level (agl) for 12 wind directions. Details of the wind climatology are shown in the wind rose presented in Figure 1d, having a mean wind speed of 6.80 m/s. Wind speed above the boundary layer was set to a value of 12 m/s based on a neutral atmosphere. In line with the study objectives of being limited to hub-height, no other conditions were imposed.

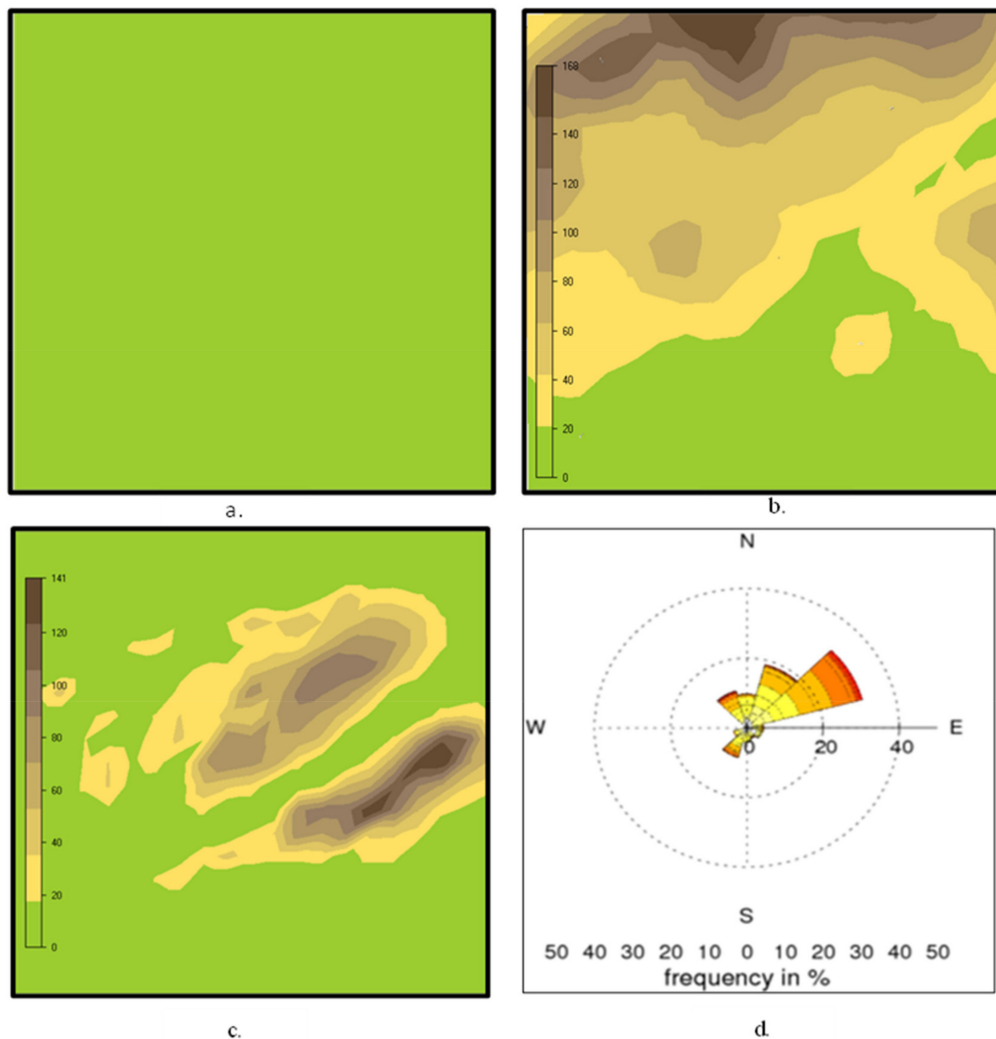


Figure 1. (a–d): Domain representation of simulations (a) offshore, (b) coastal, (c) island terrains, and (d) wind rose showing wind properties inserted at virtual climatology point.

Wind flow was obtained by iteratively solving the RANS equations for pressure; wind components u , v and w ; turbulent kinetic energy; and turbulent dissipation rate. The General Collated Velocity (GCV) solver module of WindSim was used based on the Control Volume (CV) approach to discretize the iteration solution in each control volume for a set of finite volumes. The simulations were assumed to be under a steady state atmospheric flow and turbulence, hence requiring a turbulence closure model for computation. The standard k - ϵ turbulence model (see Ferziger & Peric [40]) was applied where k and ϵ represent the turbulent kinetic energy and its dissipation rate, respectively, as expressed below:

$$\rho \frac{\delta}{\delta x_j} k \bar{u}_j = \frac{\delta}{\delta x_j} \left[\left(\frac{\mu_t}{\sigma_k} \right) \frac{\delta k}{\delta x_j} \right] + P_k - \rho \epsilon \quad (1)$$

$$\rho \frac{\delta}{\delta x_j} \epsilon \bar{u}_j = \frac{\delta}{\delta x_j} \left[\left(\frac{\mu_t}{\sigma_\epsilon} \right) \frac{\delta \epsilon}{\delta x_j} \right] + C_{\epsilon 1} P_k \frac{\epsilon}{k} - \rho C_{\epsilon 2} \frac{\epsilon^2}{k} \quad (2)$$

where μ_t represents eddy viscosity defined as:

$$\mu_t = \rho C_\mu \frac{k^2}{\epsilon} \quad (3)$$

The values 0.09, 1.44, 1.92, 1.00 and 1.30 were retained for the constants C_μ , $C_{\epsilon 1}$, $C_{\epsilon 2}$, σ_k , and σ_ϵ respectively, while P , ρ and μ represent Pressure, density and dynamic viscosity in that order. The choice of the standard k - ϵ turbulence model selection was based on its ease of adaptability to different terrains. Also, Blocken et al. [20] reported that the RANS k - ϵ turbulence model outperformed other models during a test conducted by Bechmann et al. [41] using micro-scale models for comparing wind flow resolution over Bolund hill. Turbulence intensity (TI) here is expressed as a function of turbulent kinetic energy (KE) in m^2/s^2 , wind speed scalar in the east-west direction (u_{crt}) and the north-south direction (v_{crt}) at the height being considered [42]:

$$\text{TI} = 100 \times \sqrt{\frac{\frac{4}{3} \times \text{KE}}{\sqrt{(u_{\text{crt}}^2 + v_{\text{crt}}^2)}}}} \% \quad (4)$$

Wind shear exponent is taken as the exponent α of the power law [43] also called the Hellman exponent where Z and Z_r are the wanted and reference heights respectively, while $U_{(Z)}$ and $U_{(Z)_r}$ are the wanted and reference height wind speeds respectively.

$$\frac{U_{(z)}}{U_{(z)_r}} = \left(\frac{Z}{Z_r} \right)^\alpha \quad (5)$$

The inflow angle represented by β is the angle between the wind vector and the horizontal plane while the wind speed-up is the fractional (ratio) of wind speed at the surface or crest height (due to orography) to wind speed at the same height but over a level terrain [2]. To obtain the desired hub-height properties, each terrain was refined to a mesh size of 20 m by 20 m, for 10 vertical nodes corresponding to 4000 cells. This meshing technique was deemed adequate to quantitatively illustrate changes in hub-height wind properties, although it was deemed inadequate for more detailed studies such as vertical profiles, BEM coding, aerofoil design and optimization, and general wind tunnel experimentation and simulation validation which are outside the scope of this present study.

3. Results and Discussion

3.1. Wind Fields

Spatial plots of ground-level wind field after iteration convergence are shown in Figure 2 for wind sectors 60° , 150° , 240° , and 330° . The wind speed range was least in the offshore terrain with reducing magnitude away from the wind source. The maximum wind speed recorded was less than 8.4 m/s while the minimum wind speed was greater than 7.4 m/s. Also, there is a notable absence of sheltering and funneling effects as the spatial patterns formed for the offshore terrain appear simple and homogenous. For the coastal and island terrains, wind speeds were relatively higher (between 4 m/s to 12 m/s) depending on altitude, inclination angle and wind direction. Sheltering effects were more pronounced in sectors 150° and 330° for the island simulation, forming very low wind speeds behind the crests of the hills and in depressions. Similarly for the coastal terrain, especially for the 330° sector, the wind speed was lower on the downstream side of the onshore area. Consistent with

previous studies and wind vertical profiles, the highest elevations above mean sea level had the peak wind speeds in both latter cases with values between 11–12 m/s.

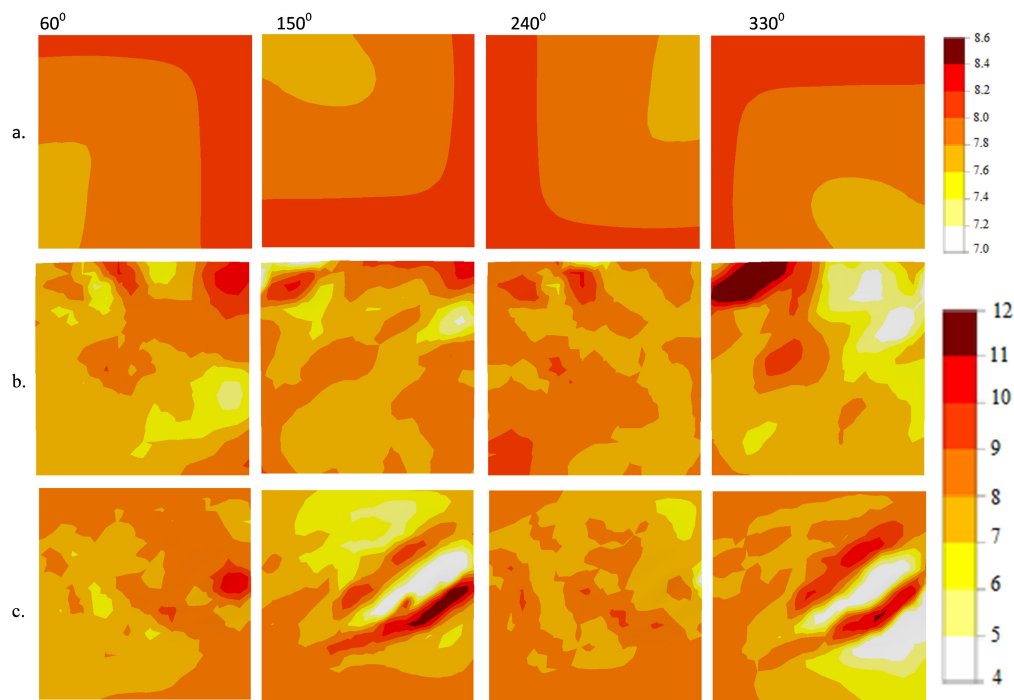


Figure 2. (a–c): Wind field values after convergence over (a) offshore, (b) coastal and (c) island terrains for wind sectors 60° , 150° , 240° , and 330° .

3.2. Turbulence Intensity

Turbulence is conventionally generated by shear and/or by thermal instability. For shear, turbulence intensity (TI) is directly proportional to the surface roughness. Hence, it is expected that TI would be least in the offshore terrain, which is obtained in the simulation here, as seen in Figure 3a. At the hub-height of 80 m above ground level (agl), offshore TI ranged from about 6–7% and could generally be classified as low turbulence [36], which is characteristic of calm open seas. For each of the wind sectors considered, TI reduced from the terrain boundary toward the mid terrain (virtual climatology point) before increasing outward thereafter. Since the offshore simulation is for a calm open sea with a constant roughness imposed on the entire terrain, the TI spatial distribution for sectors 60° and 150° appear to be mirror opposites of those of sectors 240° and 330° respectively. In terms of magnitude, a similar range of 5–7% was recorded [44] from observational data of Forschung in Nordund Ostsee 1 (FINO1) research platform, for an offshore mast located in the Island of Borkum for wind speeds between 5 m/s to 11 m/s. The results are quite different for the other two terrains, coastal and inland, as seen in Figure 3b,c respectively. TI here ranged from 4–18% depending on the incoming wind direction, orography details upstream and or downstream of the wind source, and surface roughness. For the coastal terrain, wind flow from sector 150° and 330° had the highest impact on hub-height turbulence, resulting in TI peak values of 18%. Aerodynamically, wind obstructed by “land features” from the upper (northern) boundary of the terrain may generate two effects as outlined by Emeis [2]. Shear effects come into place due to flow movement around and over the obstacle (capable of causing flow separation and reattachment), and thermal influences due to the land–sea temperature gradient. The combined effect may be more pronounced in the 330° sector than in the 150° sector, and least in the 60° sector where the TI peak value is observed offshore, upstream of the incoming wind source. A similar pattern is observed in the island terrain comprising two parallel hills running from east to west, surrounded by calm open waters. The TI in sectors 60° and 240° again appear to be mirror opposites, having lower magnitudes less than 10%, generally reducing away from wind source; the sheltering effect due to incident wind on orography is also very minimal. TI had its maximum

value at sector 150° on the crest of the higher hill, perhaps due to its characteristics. The hill which lies upstream of the incident wind has a higher altitude, steeper slope and narrower form, probably causing turbulence gained on its crest to begin to dissipate as the wind flows freely before any contact or perturbation with the crest of the lower hill. The intensities recorded here are within the range of those reported by Lubitz [36], measured on an 18 m tall tubular steel tower in a separate but related study. Nonetheless, our objective here was to illustrate using a robust approach how hub-height wind turbine aerodynamic properties can vary by terrain despite having the same properties at ground level or lower heights.

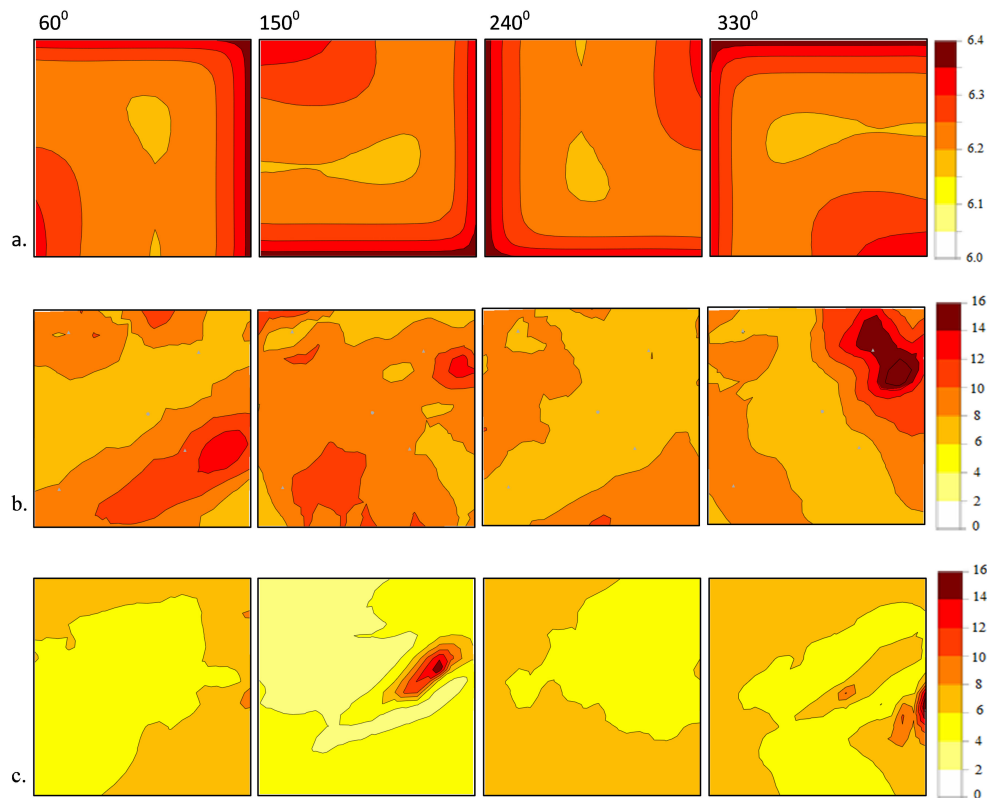


Figure 3. (a–c): Turbulence Intensity for hub-height wind flow in (a) offshore, (b) coastal and (c) island terrain simulations.

3.3. Wind Shear Exponent

Wind power assessment and prediction is usually done with hub-height wind data, which is mostly unavailable because most meteorological stations are not designed for wind energy applications [45]. Thus, extrapolating hub-height wind speed is a common practice for researchers and wind energy developers. Traditionally, the value of 0.14 is the conventional shear exponent based on the power law for wind speed extrapolation. However, there is evidence in the literature of Hellman exponent variation with surface type [43], wind speed [44], atmospheric stability [2] etc. Consequently, by examining the hub-height shear exponent for the three terrains here, we investigate the variations of the magnitude due to terrain type and the results are shown in Figure 4a–c. α ranged from about 0.08–0.10, increasing away from the wind source at the terrain border. The magnitudes compare favorably with Ray et al. [43], who reported values of 0.10 for smooth ground/ocean. The increase away from the wind source is probably best explained by the conclusions of Emeis [2] and Turk & Emeis [44] regarding the formation of waves. A combination or singular effects of wave formation, water upwelling, and land and sea-surface temperature contrast would contribute to friction between flow layers and would consequently affect wind shear reflected in the value of the exponent. For the coastal terrain, the range was relatively higher, rising to about 0.35 on crests when the wind source was

upstream, such as for sectors 150° and 330° . Lower values are also observed in the “shadowed” areas of the terrain where crests have shielded lower altitude areas on the wind flow path. A mean value between 0.12–0.18 is observed spatially, similar to field results of Turk & Emeis [44] and Drew et al. [46]. Higher values of the Hellman exponent ($\alpha > 0.4$) have been reported in meteorological measurements in Hong Kong [47], Oklahoma, USA [45], Island of Malta [48] amongst others. Actually, Blackadar [49] and Emeis [50] state that the exponent may range from 0–1. The offshore parts of the island terrain also show Hellman exponents of low magnitudes less than 0.1, which is similar to the offshore terrain for wind sector 150° and 330° , with the shadowed areas exhibiting the same characteristic. The crests here expectedly have higher values of α rising to greater than 0.30, which is also observed when wind flows from sea to land. For sectors 60° and 240° (note that legend is different due to a smaller range of values) shown in Figure 4c, the range is considerably lower at 0.04–0.18. Here the exponent was averagely less than 0.16 and seemed to increase away from the wind source, although having lower magnitudes downstream of the hills. This pattern generally agrees with the observations of the offshore terrain for both behavior away from the wind source and the magnitude. In all, the spatial variations of the Hellman exponent in wind turbine hub-height poses two challenges to wind power and turbine performance. Variations with wind direction may affect the wind vertical profile and increase the turbulence and turbine loading and by extension, blade fatigue. Secondly, estimations of wind power based on extrapolated hub-height wind speed may be inaccurate, resulting in errors. These simulations, however, broadly confirm the impact of terrain type (simple or complex) and orography on aerodynamic properties, giving insight into why and how site-specific effects are transmitted to hub-height wind characteristics.

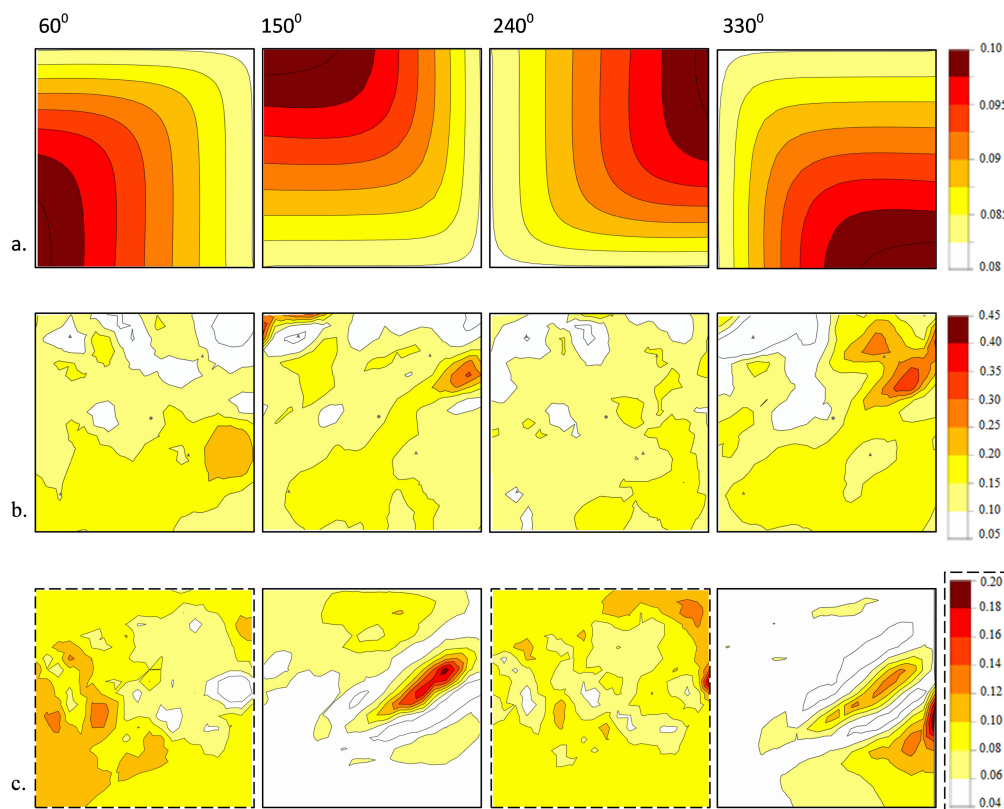


Figure 4. (a–c): Hellman Exponent for hub-height wind flow in (a) offshore, (b) coastal and (c) island terrain simulations.

3.4. Inflow Angle

The inflow angle plays a key role in turbine blade aerodynamics, and is quite relevant in blade design (Blade Element Momentum) and blade rotation. For better performance, a blade should have a

high lift-to-drag ratio. The inflow angle which is the angle formed between the wind vector and the horizontal plane can thus affect how much lift is generated by the turbine blade. The hub-height inflow angle β for the three simulated terrains are shown in Figure 5a–c with a + (positive) and – (negative) scale for below and above the horizontal. For the offshore terrain shown in Figure 5a, inflow angle is relatively constant for all wind sectors considered at less than $+1^\circ$. Aerodynamically, the incident wind is able to flow in its original path in the absence of obstacles and orography; hence, it is parallel to the horizontal. Also, since there is no wind farm set-up in the simulation, there is no wake effect present or accounted for in the initial conditions coded to the terrain. However, the coastal and island terrains in Figure 5b,c respectively have a much higher variation of about -15° to $+15^\circ$ depending on the wind source and terrain type. For the coastal terrain, the maximum inflow angle was less than $+10^\circ$, observed at the crests of the terrain. The southern boundary area also had β values slightly higher than the mid-terrain for wind sector 60° . Wind sectors 150° and 330° recorded the maximum values of inflow angle, due to the wind flow over terrain orography resulting in values as high as $+10^\circ$. One notable observation is the presence of “pockets” of very low inflow angle consequent to the shadowing effects highlighted earlier. A general decrease in β with distance away from orography is seen likewise, especially for sector 330° . The same shadowing effect is seen in the island terrain where locations upstream of the crests have inflow peaks of $+15^\circ$ before reducing to about -10° behind the crest as seen in Figure 5c for sectors 150° and 330° . For the 60° and 240° sectors, the inflow angle range was less at -10° to $+10^\circ$ and decreased away from the boundary wind source toward mid-terrain. The effects of these variations may be felt in terms of turbine blade fatigue, performance optimization and estimation error analysis. Again, we observe that orographic details play a role in wind turbine hub-height aerodynamics, corroborating the conclusions of Lydia et al. [18] regarding site-specific effects in wind turbine performance.

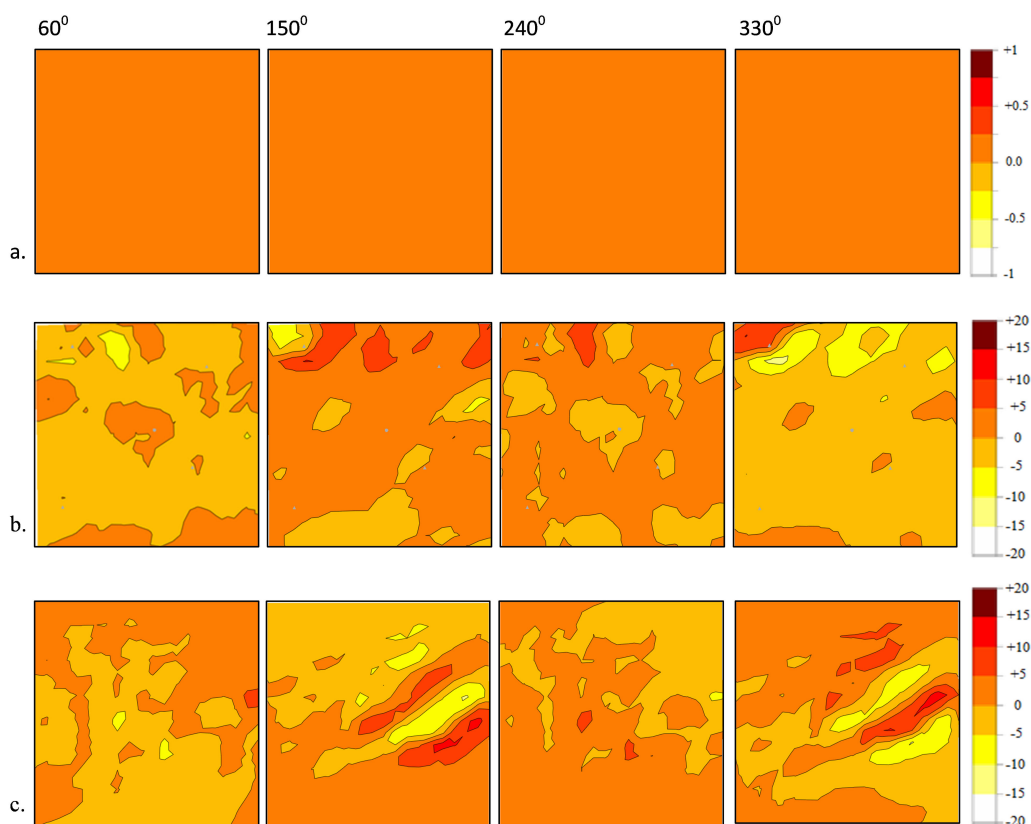


Figure 5. (a–c): Inflow angle for hub-height wind flow in (a) offshore, (b) coastal and (c) island terrain simulations.

3.5. Wind Speed-Up

Wind speed-up is an indicator of the change in selected height wind speed at a terrain crest or surface relative to the same height above ground level over a level terrain; the values for the three terrains are shown in Figure 6 for the four wind directions considered. In the coastal terrain, wind speed-up was higher in both sectors 60° and 240° at 1.13 while the value was 1.12 for sectors 150° and 330° . For all four sectors, the wind speed-up was constant in the offshore terrain at 1.08. In the island terrain sector, 330° had the least speed-up of 1.06 followed by sectors 150° , 240° and 60° with 1.07, 1.07 and 1.08 respectively. Comparatively, speed-up was maximum in the coastal terrain, which could affect the turbine in at least two ways. Firstly, the vertical profile of wind speed (with particular reference to above and below hub-height) may vary considerably, thus resulting in different gradients in both halves of the blade diameter which could then alter the overall mean wind speed across the blade. Also, extrapolation using a constant Hellman exponent to observe and model the wind profile may be erroneous due to this. Secondly, as a result of vertical profile variation, wind shear and shear-induced turbulence may be affected. If this induced turbulence is low, then the load on the turbine would be low, resulting in lower power output despite the same wind speed observed at the lower tip of the blade.

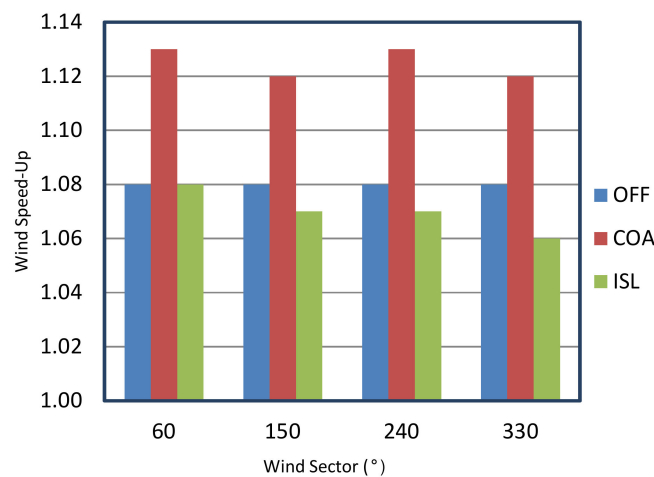


Figure 6. Observed wind speed-up at hub-height for offshore (OFF), coastal (COA) and island (ISL) terrain simulations.

When estimating the power output taking into consideration the single element model of the BEM, power output is a function of hub-height wind speed responsible for a singular lift force and a corresponding drag force. For a 2 MW Vestas V80 turbine working at a hub-height wind speed of 8 m/s, power output should be about 698 kW according to the manufacturer-supplied WTPC. Table 1 shows the estimated output (percentage increase) due to wind speed-up in each simulated terrain for the four wind directions considered. This implies that, for example, a 22% deviation of actual turbine output from the WTPC may be observed if the turbine is situated in a coastal area. The range of deviations observed here is from 17–30%, which may explain more than 60% of the reported deviations in select surveyed literature.

Here we observe two kinds of impacts. Firstly, power output from a turbine placed in any of the three terrains would differ from that of a wind tunnel with a much broader range of up to 30% as observed in the coastal simulation. Also, for each terrain, a much lower range of deviation is also possible, such as is seen here in the coastal and island simulations at 8% and 4% solely due to upstream wind direction. It is important to state here that these estimations are based on hub-height wind speed only and the single element model. This approach does not consider shear profile, TI, inflow angle, and other environmental indices.

Table 1. Percentage difference of power estimates * due to terrain effects on hub-height wind speed.

Terrain/Sector	60°	150°	240°	330°
OFF WTPC	21%	21%	21%	21%
COA WTPC	30%	22%	30%	22%
ISL WTPC	21%	19%	19%	17%

* with reference to a 2 MW WT operating at 8.0 m/s hub height wind speed in a tunnel.

4. Conclusions

The study set out to investigate and quantify the impacts of terrain type on hub-height wind aerodynamic properties relevant to wind turbine performance and power production. Wind flow over three terrains viz-a-viz offshore, coastal and island were simulated using the RANS equations for selected indices. To isolate the terrain effects, the same 40 m above mean sea level wind climatology was imposed on all three terrains, and the turbulence intensity, wind shear exponent, inflow angle and wind speed-up for four inlet directions 60°, 150°, 240° and 330° were compared.

Firstly, the wind shear exponent ranged from 0.08–0.45 depending on wind direction and terrain details. In the offshore terrain, α ranged from 0.08–0.1 with the higher values observed farther away from the wind source. A maximum value of about 0.35 was observed in the coastal terrain when wind inlet was in sector 150° and 330° due to incident wind on terrain orography details. Similarly, its value ranged from 0.04–0.45 in the island terrain with a smaller margin of 0.04–0.20 when wind direction aligned parallel to the two hills in the terrain. The maximum values were obtained on crests while the least values in troughs were shadowed by the crest altitudes. Turbulence intensity was generally less than 8% in the offshore terrain but as high as 18% for the coastal and island terrains with significant changes based on wind direction. Notably, wind sectors 330° and 150° had the higher values of TI primarily due to terrain characteristics upstream of the wind for both terrains. This resulted in a corresponding shadow effect causing lower intensities to be observed downstream in both terrains. Inflow angle remained constant at $>+1^\circ$ but had a wider range of about -15° to $+15^\circ$ in the coastal and island terrain simulations. Shadowing effects are observed behind crests, resulting in positive values of the inflow angle β especially in sector 150° for the island terrain, while the downstream trough had angles in the range of -15° to -5° . Finally, wind speed-up was maximum in the coastal terrain at 1.13 for wind directions 60° and 240°, least in the island terrain with 1.06 for wind direction 330°, but remaining constant in the offshore terrain with magnitude 1.08 irrespective of direction.

The observed variations have relevant implications for wind power as a whole. For micro-siting and resources assessment purposes, the desired location should not only consider mean wind speed at hub-height but also include at least turbulence intensity. Higher values of TI affect turbine loading and eventual power output, as well as turbine blade vulnerability to damage and failure. For power output management and optimization under the single element model of BEM, changes in inflow angle may result in changes to the lift and drag coefficients despite same wind speed. Similarly, changes in the Hellman exponent would affect vertical wind profile and mean wind speed across the turbine blade. Even in the same terrain and for the same hub-height wind speed, it is possible to have differences in power output of between 4–7% when all other factors are unchanged. Relative to a tunnel-tested 2 MW WT power output, site-specific effects related to terrain type may only account for up to 30% of the difference observed. Advancing the results of this study would require the collection and use of operational WT data not limited to wind speed only, while exploring the vertical profiles of the explored properties that motivate future research simulation and study.

Author Contributions: The study idea, plan and design was conceived by W.Z. and A.T.A., while the simulations, visualizations and analysis were carried out by A.T.A. and W.Z. All authors jointly prepared the manuscript and decided on the final version. **Funding** The first author is a recipient of a research studentship provided by the City University of Hong Kong.

Acknowledgments: The authors would like to thank the WindSim Company, Sales Team and Online Technical Support Team whose software was extensively used for the terrain modifications and simulations in this study. Special thanks to the Ceetron team and the Hong Kong Observatory. We are also grateful to the anonymous reviewers for their insightful comments, which helped improve the overall quality of this publication.

Conflicts of Interest: The authors declare no conflict of interest

References

1. Kusiak, A. Share data on wind energy: Giving researchers access to information on turbine performance would allow wind farms to be optimized through data mining. *Nature* **2016**, *529*, 19–22. [[CrossRef](#)] [[PubMed](#)]
2. Emeis, S. Current issues in wind energy meteorology. *Meteorol. Appl.* **2014**, *21*, 803–819. [[CrossRef](#)]
3. Cetinay, H.; Kuipers, F.A.; Guven, A.N. Optimal siting and sizing of wind farms. *Renew. Energy* **2017**, *101*, 51–58. [[CrossRef](#)]
4. Gao, X.; Yang, H.; Lu, L. Study on offshore wind power potential and wind farm optimization in Hong Kong. *Appl. Energy* **2014**, *130*, 519–531. [[CrossRef](#)]
5. Yu, L.; Zhong, S.; Bian, X.; Heilman, W.E. Climatology and trend of wind power resources in China and its surrounding regions: A revisit using Climate Forecast System Reanalysis data. *Int. J. Climatol.* **2016**, *36*, 2173–2188. [[CrossRef](#)]
6. Wang, Y.; Liu, Y.; Li, L.; Infield, D.; Han, S. Short-Term Wind Power Forecasting Based on Clustering Pre-Calculated CFD Method. *Energies* **2018**, *11*, 854. [[CrossRef](#)]
7. Konopka, J.; Lopes, A.; Matzarakis, A. An Original Approach Combining CFD, Linearized Models, and Deformation of Trees for Urban Wind Power Assessment. *Sustainability* **2018**, *10*, 1915. [[CrossRef](#)]
8. Di Sabatino, S.; Buccolieri, R.; Salizzoni, P. Recent advancements in numerical modelling of flow and dispersion in urban areas: A short review. *Int. J. Environ. Pollut.* **2013**, *7*, 172–191. [[CrossRef](#)]
9. Blocken, B. 50 years of computational wind engineering: Past, present and future. *J. Wind Eng. Ind. Aerodyn.* **2014**, *129*, 69–102. [[CrossRef](#)]
10. Yan, S.; Shi, S.; Chen, X.; Wang, X.; Mao, L.; Liu, X. Numerical simulations of flow interactions between steep hill terrain and large scale wind turbine. *Energy* **2018**, *151*, 740–747. [[CrossRef](#)]
11. Toparlar, Y.; Blocken, B.; Vos, P.; Van Heijst, G.J.F.; Janssen, W.D.; van Hooff, T.; Montazeri, H.; Timmermans, H.J.P. CFD simulation and validation of urban microclimate: A case study for Bergpolder Zuid, Rotterdam. *Build. Environ.* **2015**, *83*, 79–90. [[CrossRef](#)]
12. Sanderse, B.; Pijl, S.P.; Koren, B. Review of computational fluid dynamics for wind turbine wake aerodynamics. *Wind Energy* **2011**, *14*, 799–819. [[CrossRef](#)]
13. Shakoor, R.; Hassan, M.Y.; Raheem, A.; Wu, Y.K. Wake effect modeling: A review of wind farm layout optimization using Jensen's model. *Renew. Sustain. Energy Rev.* **2016**, *58*, 1048–1059. [[CrossRef](#)]
14. Hansen, K.S.; Barthelmie, R.J.; Jensen, L.E.; Sommer, A. The impact of turbulence intensity and atmospheric stability on power deficits due to wind turbine wakes at Horns Rev wind farm. *Wind Energy* **2012**, *15*, 183–196. [[CrossRef](#)]
15. Gahi, M.H.; Dehkordi, A.J. Investigating the influence of dimensional scaling on aerodynamic characteristics of wind turbine using CFD simulation. *Renew. Energy* **2016**, *97*, 162–168. [[CrossRef](#)]
16. Cai, X.; Gu, R.; Pan, P.; Zhu, J. Unsteady aerodynamics simulation of a full-scale horizontal axis wind turbine using CFD methodology. *Energy Convers. Manag.* **2016**, *112*, 146–156. [[CrossRef](#)]
17. Alaimo, A.; Esposito, A.; Messineo, A.; Orlando, C.; Tumino, D. 3D CFD analysis of a vertical axis wind turbine. *Energies* **2015**, *8*, 3013–3033. [[CrossRef](#)]
18. Zanon, A.; De Gennaro, M.; Kühnelt, H. Wind energy harnessing of the NREL 5 MW reference wind turbine in icing conditions under different operational strategies. *Renew. Energy* **2018**, *115*, 760–772. [[CrossRef](#)]
19. Dhunny, A.Z.; Lollchund, M.R.; Rughooputh, S.D.D.V. Wind energy evaluation for a highly complex terrain using Computational Fluid Dynamics (CFD). *Renew. Energy* **2017**, *101*, 1–9. [[CrossRef](#)]
20. Blocken, B.; van der Hout, A.; Dekker, J.; Weiler, O. CFD simulation of wind flow over natural complex terrain: Case study with validation by field measurements for Ria de Ferrol, Galicia, Spain. *J. Wind Eng. Ind. Aerodyn.* **2015**, *147*, 43–57. [[CrossRef](#)]
21. Cooney, C.; Byrne, R.; Lyons, W.; O'Rourke, F. Performance characterisation of a commercial-scale wind turbine operating in an urban environment, using real data. *Energy Sustain. Dev.* **2017**, *36*, 44–54. [[CrossRef](#)]

22. Long, H.; Wang, L.; Zhang, Z.; Song, Z.; Xu, J. Data-driven wind turbine power generation performance monitoring. *IEEE Trans. Ind. Electron.* **2015**, *62*, 6627–6635. [[CrossRef](#)]
23. Staffell, I.; Green, R. How does wind farm performance decline with age? *Renew. Energy* **2014**, *66*, 775–786. [[CrossRef](#)]
24. Abolude, A.; Zhou, W. Assessment and Performance Evaluation of a Wind Turbine Power Output. *Energies* **2018**, *11*, 1992. [[CrossRef](#)]
25. Bludszuweit, H.; Domínguez-Navarro, J.A.; Llombart, A. Statistical analysis of wind power forecast error. *IEEE Trans. Power Syst.* **2008**, *23*, 983–991. [[CrossRef](#)]
26. Carrillo, C.; Montaña, A.O.; Cidrás, J.; Díaz-Dorado, E. Review of power curve modelling for wind turbines. *Renew. Sustain. Energy Rev.* **2013**, *21*, 572–581. [[CrossRef](#)]
27. Schlechtingen, M.; Santos, I.F.; Achiche, S. Using data-mining approaches for wind turbine power curve monitoring: A comparative study. *IEEE Trans. Sustain. Energy* **2013**, *4*, 671–679. [[CrossRef](#)]
28. Shokrzadeh, S.; Jozani, M.J.; Bibeau, E. Wind turbine power curve modeling using advanced parametric and nonparametric methods. *IEEE Trans. Sustain. Energy* **2014**, *5*, 1262–1269. [[CrossRef](#)]
29. Villanueva, D.; Feijóo, A. Normal-based model for true power curves of wind turbines. *IEEE Trans. Sustain. Energy* **2016**, *7*, 1005–1011. [[CrossRef](#)]
30. Whale, J.; McHenry, M.P.; Malla, A. Scheduling and conducting power performance testing of a small wind turbine. *Renew. Energy* **2013**, *55*, 55–61. [[CrossRef](#)]
31. Li, S.; Wunsch, D.C.; O’Hair, E.A.; Giesselmann, M.G. Using neural networks to estimate wind turbine power generation. *IEEE Trans. Energy Convers.* **2001**, *16*, 276–282.
32. Lydia, M.; Kumar, S.S.; Selvakumar, A.I.; Kumar, G.E.P. A comprehensive review on wind turbine power curve modeling techniques. *Renew. Sustain. Energy Rev.* **2014**, *30*, 452–460. [[CrossRef](#)]
33. Jafarian, M.; Ranjbar, A.M. Fuzzy modeling techniques and artificial neural networks to estimate annual energy output of a wind turbine. *Renew. Energy* **2010**, *35*, 2008–2014. [[CrossRef](#)]
34. Zamani, M.H.; Riahy, G.H.; Ardakani, A.J. Modifying power curve of variable speed wind turbines by performance evaluation of pitch-angle and rotor speed controllers. In Proceedings of the 2007 IEEE Canada Electrical Power Conference, Montreal, QC, Canada, 25–26 October 2007; pp. 347–352.
35. Tindal, A.; Johnson, C.; LeBlanc, M.; Harman, K.; Rareshide, E.; Graves, A. Site-specific adjustments to wind turbine power curves. In Proceedings of the AWEA Wind Power Conference, Houston, TX, USA, 4 June 2008.
36. Lubitz, W.D. Impact of ambient turbulence on performance of a small wind turbine. *Renew. Energy* **2014**, *61*, 69–73. [[CrossRef](#)]
37. Uchida, T. LES Investigation of Terrain-Induced Turbulence in Complex Terrain and Economic Effects of Wind Turbine Control. *Energies* **2018**, *11*, 1530. [[CrossRef](#)]
38. Bilal, M.; Birkelund, Y.; Homola, M.; Virk, M.S. Wind over complex terrain—Microscale modelling with two types of mesoscale winds at Nygårdsfjell. *Renew. Energy* **2016**, *99*, 647–653. [[CrossRef](#)]
39. Dhunny, A.Z.; Lollchund, M.R.; Rughooputh, S.D.D.V. Numerical analysis of wind flow patterns over complex hilly terrains: Comparison between two commonly used CFD software. *Int. J. Glob. Energy Issues* **2016**, *39*, 181–203. [[CrossRef](#)]
40. Ferziger, J.H.; Peric, M. *Computational Methods for Fluid Mechanics*; Springer: Berlin, Germany, 2002.
41. Bechmann, A.; Sørensen, N.N.; Berg, J.; Mann, J.; Réthoré, P.E. The Bolund experiment, part II: Blind comparison of microscale flow models. *Bound.-Lay. Meteorol.* **2011**, *141*, 245. [[CrossRef](#)]
42. WindSim WindSim Manual Sourced. Available online: <https://www.windsim.com/products/windsim-brochures.aspx> (accessed on 24 December 2017).
43. Ray, M.L.; Rogers, A.L.; McGowan, J.G. *Analysis of Wind Shear Models and Trends in Different Terrains*; Renewable Energy Research Laboratory, Department of Mechanical & Industrial Engineering, University of Massachusetts: Amherst, MA, USA, 2006.
44. Türk, M.; Emeis, S. The dependence of offshore turbulence intensity on wind speed. *J. Wind Eng. Ind. Aerodyn.* **2010**, *98*, 466–471. [[CrossRef](#)]
45. Newman, J.F.; Klein, P.M. The impacts of atmospheric stability on the accuracy of wind speed extrapolation methods. *Resources* **2014**, *3*, 81–105. [[CrossRef](#)]
46. Drew, D.R.; Barlow, J.F.; Lane, S.E. Observations of wind speed profiles over Greater London, UK, using a Doppler lidar. *J. Wind Eng. Ind. Aerodyn.* **2013**, *121*, 98–105. [[CrossRef](#)]

47. Shu, Z.R.; Li, Q.S.; He, Y.C.; Chan, P.W. Observations of offshore wind characteristics by Doppler-LiDAR for wind energy applications. *Appl. Energy* **2016**, *169*, 150–163. [[CrossRef](#)]
48. Farrugia, R.N. The wind shear exponent in a Mediterranean island climate. *Renew. Energy* **2003**, *28*, 647–653. [[CrossRef](#)]
49. Blackadar, A.K. *Turbulence and Diffusion in the Atmosphere*; Springer: Berlin, Germany, 1997.
50. Emeis, S. *Wind Energy Meteorology*; Springer: Berlin, Germany, 2013.



© 2018 by the authors. Licensee MDPI, Basel, Switzerland. This article is an open access article distributed under the terms and conditions of the Creative Commons Attribution (CC BY) license (<http://creativecommons.org/licenses/by/4.0/>).